ELSEVIER

Journal of Alloys and Compounds 444–445 (2007) 410–414

Journal of ALLOYS AND COMPOUNDS

www.elsevier.com/locate/jallcom

# XAS study of $(U_{1-y}Pu_y)O_2$ solid solutions

P. Martin [a,*], S. Grandjean [b], C. Valot [a], G. Carlot [a], M. Ripert [a], P. Blanc [b], C. Hennig [c]

[a] *CEA Cadarache, DEN/DEC/SESC, bât. 151, 13108 St Paul Lez Durance Cedex, France*
[b] *CEA Marcoule, DEN/DRCP/SCPS, BP 171, 30270 Bagnols sur Cèze Cedex, France*
[c] *Forschungszentrum Rossendorf, Institute of Radiochemistry, P.O. Box 510119, 01314 Dresden, Germany*

Received 28 June 2006; received in revised form 20 December 2006; accepted 5 January 2007
Available online 14 January 2007

**Abstract**

A new procedure for $(U,Pu)O_2$ nuclear fuel manufacturing based on the oxalic coprecipitation of U(IV) and Pu(III) followed by the thermal conversion of the coprecipitate into oxide is under development. In order to fully investigate the ideality of solid solution with Pu content equal to 50, 30, 15 and 7 at.%, X-ray powder diffraction (XRD) and X-ray absorption spectroscopy (XAS) characterizations at uranium and plutonium $L_{III}$ edges have been undertaken. Using XRD, a face centred cubic structure was observed in each case, and the cell parameter deduced follows satisfactorily the Vegard's law. However, extended X-ray absorption fine structure (EXAFS) measurements moderate these results; only the $(U_{0.5}Pu_{0.5})O_2$ sample leads to the same conclusion as XRD. For the lower plutonium concentration, a disordered hyperstoichiometric structure $(U_{1-y}Pu_y)O_{2+x}$ has been revealed. In those compounds, cuboctahedral oxygen defects are only located around uranium atoms and not in the Pu environment. A much more complex structure than that suggested by the XRD is thus observed with a non-random distribution of plutonium atoms within the uranium sites of the $(U_{1-y}Pu_y)O_{2+x}$ structure.


*Keywords:* Actinide alloys and compounds; Extended X-ray absorption fine structure (EXAFS); Oxide materials; Solid state reactions

## 1. Introduction

The plutonium generated in nuclear power reactors can be reprocessed, at least partially, through the use of a mixed oxide (MOX) $(U,Pu)O_2$ fuel. MOX fuel is manufactured industrially by cocrushing, pelletizing and sintering of $UO_2$ and $PuO_2$ powders. A fluorite type solid solution $(U,Pu)O_2$ is obtained using this method. Currently, rather than a mechanical mixing of pulverulent compounds, a new manufacturing technique based on a coprecipitation of uranium and plutonium (chemical mixture) is under development. A better homogeneity of the U and Pu repartition in the solid is expected by this "wet route". The homogeneity of the final products may be a significant criterion for an optimized behavior in power reactors. This synthesis method currently being developed in the CEA Atalante facility at Marcoule [1,2], is based on the oxalic coprecipitation of U(IV) and Pu(III) followed by the thermal conversion of the coprecipitate into oxide. The goal is to obtain $(U,Pu)O_2$ solid solutions with a minimal content of synthesis impurities and an oxygen to metal ratio (O/M) equal to 2.0.

The lattice parameter of $U_{1-y}Pu_yO_2$ solid solution is known to change linearly with $y$ from pure $UO_2$ to pure $PuO_2$. This feature is commonly referred to as Vegard's law. Usually, solid solution structures are studied using diffraction methods. But, as pointed out by Purans et al. [3], in order to fully investigate the ideality of a solid solution, a more local probe is needed. X-ray absorption spectroscopy (XAS) using synchrotron radiation is an extremely suitable technique to study local atomic and electronic structures of mixed actinide oxides [3,4] such as $U_{1-y}Pu_yO_2$.

## 2. Experimental methods

### 2.1. The preparation of $(U_{1-y}Pu_y)O_2$ solid solutions

$(U,Pu)O_2$ solid solutions were prepared by oxalic coconversion via coprecipitation of U(IV) and Pu(III) under controlled conditions in order to obtain mixed U(IV)–Pu(III) single oxalic phases [5]. Four Pu(III)/U(IV) molar ratios were studied: 7/93, 15/85, 30/70 and 50/50.

The uranium(IV) solution was obtained by catalytic reduction of a uranyl nitrate solution under $H_2$ pressure in a closed reactor using hydrazinium nitrate as stabilizer. The plutonium(IV) solution was prepared by dissolving the standard

* Corresponding author. Tel.: +33 4 42 25 38 66; fax: +33 4 42 25 32 85.
*E-mail address:* martinp@drncad.cea.fr (P. Martin).

0925-8388/$ – see front matter © 2007 Elsevier B.V. All rights reserved.
doi:10.1016/j.jallcom.2007.01.032

Table 1
Evolution of the cell parameter $a$ with Pu content in $(U,Pu)O_2$ solid solution $a$ measured by XRD and calculated using Vegard's law, and the first three calculated coordination shell distances (all values are in Å)

| $y$ (at.% Pu) | $a$ (XRD) | $a$ (Vegard's law) | First shell metal–O | Second shell metal–metal | Third shell metal–O |
|---|---|---|---|---|---|
| 0 | 5.470(2) | 5.47 | 2.369 | 3.868 | 4.535 |
| 7 | 5.465(2) | 5.4648 | 2.367 | 3.864 | 4.532 |
| 15 | 5.457(2) | 5.4589 | 2.363 | 3.858 | 4.524 |
| 30 | 5.444(2) | 5.4478 | 2.357 | 3.849 | 4.514 |
| 50 | 5.434(2) | 5.4330 | 2.353 | 3.842 | 4.506 |
| 100 | 5.398(2) | 5.3960 | 2.337 | 3.817 | 4.475 |

dioxide in hydrofluoric-nitric acid and purifying the obtained solution on an ion-exchange resin. Plutonium was subsequently adjusted to the trivalent state by slowly adding a 7 M hydrazinium nitrate solution to the Pu(IV) solution by stirring and gentle warming (60 °C) until a final excess concentration of 0.1 M hydrazinium ions is reached. All of the experiments were performed with ultrapure water (18 MΩ cm) provided by a Milli Q purification system (Millipore).

For each experiment, the oxalate coprecipitate was prepared by mixing a solution of U(IV) and Pu(III) and a concentrated $H_2C_2O_4$ solution (with a slight excess of $H_2C_2O_4$) in an acidic medium containing a single-charged cation (such as the ion hydrazinium).

The resulting crystallized powder was filtered off, washed with an aqueous solution of nitric acid and oxalic acid, and dried at room temperature. The actinide loss during the coprecipitation step was less than 0.5%.

Each coprecipitate was then thermally treated up to 950 °C using a 10 °C/min gradient and under an argon flow in order to obtain the mixed $(U,Pu)O_2$ oxide phase. $UO_2$ and $PuO_2$ reference compounds were synthesized following the same chemical procedure. In each sample, the oxygen/metal ratio was measured using thermo-gravimetric analysis and was equal to $2.00 \pm 0.02$.

For the extended X-ray absorption fine structure (EXAFS) investigations, 10–20 mg of the oxide powder was diluted with cellulose and the resulting mixture was pressed.

### 2.2. Apparatus and analytical methods

X-ray powder diffraction (XRD) data were obtained with an INEL CPS 120 diffractometer (curved position sensitive detector) using Cu $K\alpha_1$ radiation isolated by a germanium monochromator. Gold was added to each oxide sample as an internal standard in order to calibrate the angular positions of the diffraction lines observed.

XAS measurements were performed on the ROBL beam line of the European Synchrotron Radiation Facility (Grenoble, France). For each sample, XAS spectra were recorded at uranium and plutonium $L_{III}$ edges in transmission mode except for low plutonium concentration samples (7% and 15%). In those cases, Pu spectra were collected using a 4 elements fluorescence detector. Energy calibrations of the X-ray absorption near edge structure (XANES) data were achieved using the Y foil (17.038 keV) and Zr foil (17.998 keV) references positioned after the second ionisation chamber. ATHENA software [6] was used for extracting EXAFS oscillations from the raw absorption spectra. Metric parameters (neighbouring atomic distances ($R$), mean squared radial displacement or Debye–Waller factors ($\sigma^2$) and coordination numbers ($N$)) were obtained from the EXAFS data using ARTEMIS[6] software with FEFF8.20 [7] calculations. Experimental EXAFS spectra were Fourier transformed using a Sine window over a $k$ space range of 3–14.5 $Å^{-1}$ range for both plutonium and uranium. Curve fitting was performed in $k^3$ for $R$-values in the range 1.3–4.3 Å. The overall quality and suitability of the fit is evaluated by ARTEMIS and is shown as the "$R$-factor" in Table 2. A value of 0.02 signifies that the average deviation between the theory and the data is two percent. During the fitting process, the amplitude factor ($S_2^0$) was fixed at 0.9 [8], and $E_0$ were fixed to values obtained on reference samples $UO_2$ and $PuO_2$.

## 3. Results

The $(U,Pu)O_2$ samples were analyzed by XRD, along with the $UO_2$ and $PuO_2$ reference compounds. The lattice parameter of each oxide was refined by pattern matching using the FullProf software [9]. In each case, a face centred cubic structure was observed and the deduced cell parameters suitably follow the Vegard's law as seen in Table 1. These results confirm the obtaining of solid solutions $(U,Pu)O_2$. Following the oxalic coprecipitation and the subsequent thermal treatment, the mixing of U and Pu in the oxide is then achieved at a submicronic scale before the sintering step. However, the limitations of the XRD investigations impede a more quantitative conclusion concerning the local homogeneity of the U and Pu repartition in the oxide.

The evolutions of the Fourier transforms are summarized in Figs. 1 and 2. For both actinides, the overall shape of the spectra remains the same with two main peaks located at ~2 Å (corresponding to the first An–O coordination shell) and ~4 Å (corresponding to the An–An shell and second An–O shell). But a significant decrease of the second peak intensity is observed in samples with a Pu content of less than 50%. Furthermore, An–O first coordination shells display an unexpected behaviour:

- for plutonium, an apparent decrease of the Pu–O bond length is observed. Based on the Vegard's law values given in Table 1, an increase of Pu–O bonds was expected;
- for uranium, a distortion of the peak can be seen in samples with less than 50 at.% of Pu.

Therefore, a more complex local environment of both actinides than suggested by the Vegard's law is observed.

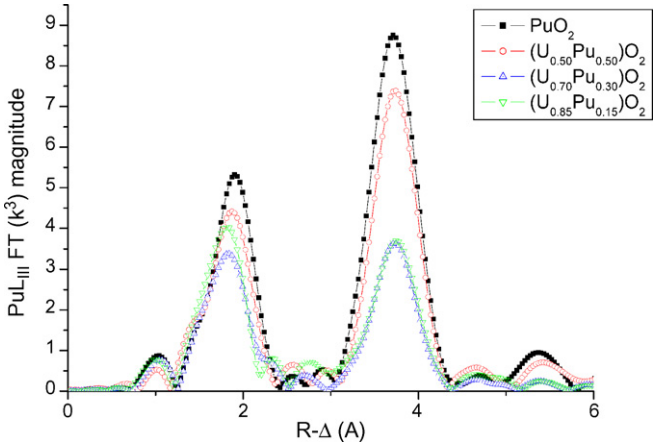


Fig. 1. Fourier transforms at the Pu $L_{III}$ edge.

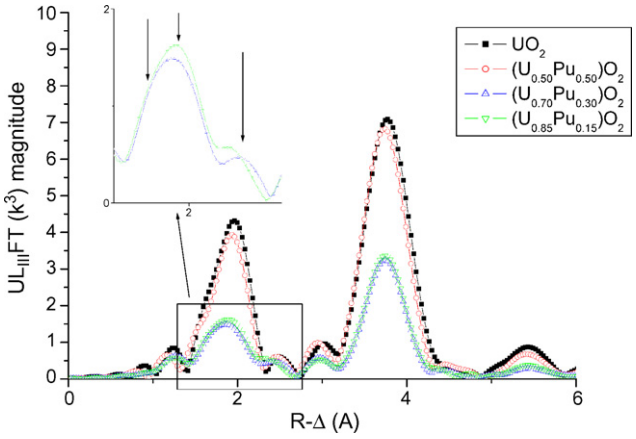


Fig. 2. Fourier transforms at the U $L_{III}$ edge. For $(U_{0.70}Pu_{0.30})O_2$ and $(U_{0.85}Pu_{0.15})O_2$ samples, an enlargement of the first coordination shell (U–O bonds) is shown, the three arrows indicate the three U–O bonds needed to fit spectra.

### 3.1. X-ray absorption near edge structure (XANES)

As XANES is very sensitive to both the oxidation state and change in the local geometry, spectra collected at both edges could help us to understand Fourier transform evolutions. At the Pu $L_{III}$ edge, whatever the Pu content, the XANES spectra remain identical to the signal observed for $PuO_2$. Plutonium atoms thus remain Pu(IV) in a cubic symmetry.

In the uranium case, as shown in Fig. 3, a white line position shift toward higher energy coupled with an increase in intensity of the shoulder located at ∼17.190 eV can be noted, except for the $(U_{0.5}Pu_{0.5})O_2$ sample which is identical to the spectra collected on $UO_2$. Such behavior is characteristic of a presence of hyperstoichiometric $UO_2$ structure ($UO_{2+x}$) as presented by Conradson et al. [10]. Therefore, based on XANES interpretation, in solid solution with $y$ equal to 30, 15 and 7, a hyperstoichiometric structure is observed around uranium ions while the plutonium environment remains identical to the $PuO_2$ one.

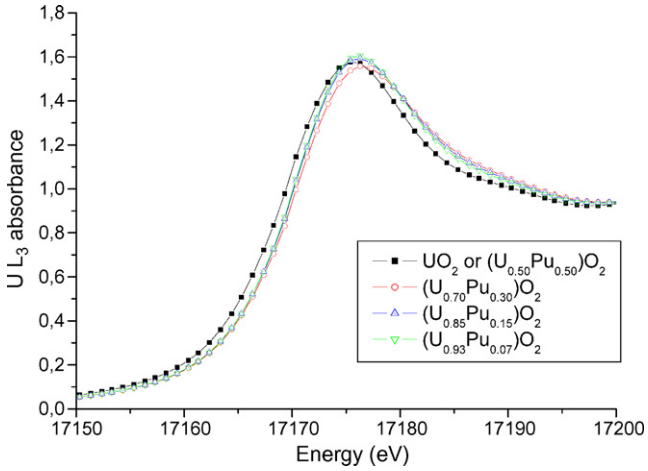


Fig. 3. Uranium $L_{III}$ XANES of $(U_{1-y},Pu_y)O_2$ solid solutions.

### 3.2. Extended X-ray absorption fine structure (EXAFS)

Metric parameters extracted from EXAFS data at both edges (given in Table 2) confirm the XANES interpretation. At the uranium edge, the first coordination shell (U–O) can be reproduced with one distance only for the $(U_{0.5}Pu_{0.5})O_2$ sample.

For the $(U_{0.5}Pu_{0.5})O_2$ sample, the uranium local environment is clearly the one of an ideal stoichiometric solid solutions, since bond lengths are equal to values calculated in Table 1. The case of the plutonium environment is slightly more complicated. As mentioned before, the Pu–O first distance decreases with uranium content whereas the contrary is expected (Table 1). Furthermore, as seen on Fig. 1, the shape of this peak (first coordination shell) is no longer gaussian. To reproduce it, we had to introduce an additional asymmetry term (third cumulant) [11]. Using this method, we finally obtained a shell of eight oxygen atoms at a distance of 2.351(5) Å, which is consistent with the result obtained at the uranium edge. Regarding the plutonium–metal shell, we also found an ideal solid solution structure with Pu–Pu and Pu–U distances equal to 3.845(5) Å. The results of the analysis at the two edges clearly show that the chemical procedure used to manufacture the $(U_{0.5}Pu_{0.5})O_2$ sample is validated.

For the other concentrations, as revealed by the uranium $L_{III}$ edge XANES spectra, the U–O first shell can no longer be modeled with only one distance. Three distinct U–O distances are needed to reproduce the experimental data: around the "fluorite" distance ∼2.36 Å, a shorter one at 2.25 Å and a longer one at ∼2.86 Å. These three distances are represented by arrows in the enlargement of the U–O shells shown in Fig. 2 (the peaks occur at shorter distances because the figure is not corrected for phase shift). These distances are in accordance with the recent description of the $UO_{2+x}$ structure [12–14]. This description is based on the presence of cuboctahedral defects into the fluorite structure. The particularity of this evolution is that uranium atoms remain into their fluorite position (0, 0, 0), whereas several new oxygen positions, slightly shifted from the (0.25, 0.25, 0.25) position, enter the fluorite structure. This behavior leads to some reduced U–O bond lengths ∼0.15 Å balanced by the expansion of others and an increase in the U coordination numbers [14]. Both bond lengths and neighboring numbers obtained for the 30, 15 and 7% samples are in accordance with the cuboctahedral model. Such observations, confirm the fact that a local hyperstoichiometry is observed around uranium atoms for those samples. It must be pointed out that no uranyl type short distance (∼1.8 Å) as observed by Conradson et al. [10] on $UO_{2+x}$ samples has been observed in our EXAFS data.

On the other hand, the plutonium environments are not disturbed by the hyperstoichoimetry: except for the introduction of a third cumulant in the first shell for all the samples, no evidence of any other Pu–O distances is observed. Experimental data can be modeled with a single Pu–O distance. Therefore, the oxygen defects revealed at uranium edge are not homogeneously distributed into the $(U,Pu)O_{2+x}$ structure. This conclusion is consistent with the fact that under our thermal conditions only $PuO_2$ is stable [15]. Thus, the excess charge due to additional oxygen atoms is only supported by the ura-

Table 2
Metric parameters extracted by fitting of EXAFS spectra measured at U and Pu $L_{III}$ edges for $(U_{1-y}Pu_y)O_2$ samples and $UO_2$ and $PuO_2$ reference compounds

| $y$ (at.% Pu) | Edge | Shell | $R$ (Å) | $N$ | $\sigma^2$ (Å$^2$) | $R$-factor |
|---|---|---|---|---|---|---|
| 100 | Pu | O | 2.333(5) | 8.0(5) | 0.0064(5) | 0.005 |
| | | Pu | 3.820(5) | 12.0(5) | 0.0033(3) | |
| | | O | 4.48(2) | 24(2) | 0.010(2) | |
| 50 | Pu | O | 2.351 (5) | 8.0(5) | 0.0081(5) | 0.012 |
| | | Pu and U | 3.845(5) | 12 | 0.0030(3) | |
| | | O | 4.52 (2) | 24(2) | 0.013(2) | |
| | U | O | 2.352(5) | 8.1(5) | 0.0073(5) | 0.017 |
| | | Pu and U | 3.845(5) | 12 | 0.0054(3) | |
| | | O | 4.51(2) | 24(2) | 0.013(2) | |
| 30 | Pu | O | 2.353(5) | 7.7(5) | 0.0098(5) | 0.016 |
| | | Pu and U | 3.845(5) | 12 | 0.0045(5) | |
| | | O | 4.47(2) | 23(2) | 0.020(2) | |
| | U | O | 2.28(1) | 1.1(5) | 0.0067(5) | 0.007 |
| | | O | 2.35(1) | 6.5(5) | 0.019(1) | |
| | | O | 2.85(1) | 0.7(5) | 0.0056(5) | |
| | | Pu and U | 3.858(5) | 12 | 0.0065(5) | |
| | | O | 4.53(2) | 18(2) | 0.015(2) | |
| 15 | Pu | O | 2.351(5) | 8.0(5) | 0.0088(5) | 0.02 |
| | | Pu and U | 3.857(5) | 12 | 0.0058(5) | |
| | | O | 4.49(2) | 24(2) | 0.019(2) | |
| | U | O | 2.28(1) | 1.0(5) | 0.0064(5) | 0.005 |
| | | O | 2.36(1) | 6.7(5) | 0.017(1) | |
| | | O | 2.84(1) | 1.0(5) | 0.0070(5) | |
| | | Pu and U | 3.865(5) | 12 | 0.0063(5) | |
| | | O | 4.54(2) | 18(2) | 0.015(2) | |
| 7 | Pu | O | 2.366(5) | 8.1(5) | 0.0090(5) | 0.02 |
| | | Pu and U | 3.868(5) | 12 | 0.0060(5) | |
| | | O | 4.52(2) | 24(2) | 0.020(2) | |
| | U | O | 2.31(1) | 1.2(5) | 0.0050(5) | 0.01 |
| | | O | 2.36(1) | 6.7(5) | 0.014(1) | |
| | | O | 2.86(1) | 1.1(5) | 0.0070(5) | |
| | | Pu and U | 3.868(5) | 12 | 0.0051(5) | |
| | | O | 4.56(2) | 18(2) | 0.014(2) | |
| 0 | U | O | 2.370(5) | 8.0(5) | 0.0080(5) | 0.015 |
| | | U | 3.865(5) | 12.0(5) | 0.0050(5) | |
| | | O | 4.53(2) | 24(2) | 0.007(2) | |

nium ions, as pointed out by the XANES results. Furthermore, this observation confirmed the anisotropy of plutonium oxygen shell revealed in the fitting process by the introduction of the third cumulant.

As for the metal–metal shells, at both edges and for all samples, distances are in accordance with values calculated using the Vegard's law. But an increase of the Debye–Waller factors has been observed, indicating a more disordered structure. Such behavior can be directly attributed to the presence of an hyperstoichiometric solid solution.

## 4. Conclusion

By combining XRD and XAS at uranium and plutonium $L_{III}$ edges, we have been able to confirm the precipitation of solid solutions $(U,Pu)O_2$ using the new "wet route" process. However, for a Pu content less or equal to 30%, a disordered hyperstoichiometric structure $(U_{1-y}Pu_y)O_{2+x}$ has been revealed. In these compounds, cuboctahedral oxygen defects are only located around uranium atoms and not in the Pu environment. A much more complex structure than that suggested by the XRD is thus observed with a non-random distribution of plutonium atoms into the uranium sites of the $(U_{1-y}Pu_y)O_{2+x}$ structure.

Current optimizations of the preparation method aim at precisely controlling each step of the decomposition of the mixed oxalate compound up to the oxide phase, in order to correlate the reaction pathway during synthesis with the local disorder observed by the EXAFS investigation on the $(U,Pu)O_2$ solid solutions (for Pu content less or equal to 30%). Complex redox mechanisms during decomposition, involving at least the plutonium but also the uranium, could indeed affect the local order around the metal even in the final oxide phase. Further EXAFS investigations are planned with new optimized samples.

## References

[1] S. Grandjean, B. Chapelet-Arab, S. Lemonnier, A.-C. Robisson, N. Vigier, Actinides—Basic Science Applications and Technology Symposium, MRS Fall Meeting, 26 November–2 December, Boston, 2005.
[2] S. Grandjean, A.C. Robisson, J. Dauby, S. Picart, M. Lecomte, M. Masson, P. Brossard, GLOBAL 2005, Proceeding No. 122, October 9–13, Tsukuba, Japan, 2005.
[3] J. Purans, G. Heisbourg, N. Dacheux, P. Moisy, S. Hubert, Phys. Scr. 115 (2005) 925–927.
[4] P. Martin, M. Ripert, T. Petit, T. Reich, C. Hennig, F. D'Acapito, J.L. Hazemann, O. Proux, J. Nucl. Mater. 312 (2003) 103–110.
[5] B. Arab-Chapelet, S. Grandjean, G. Nowogrocki, F. Abraham, J. Alloys Compd. 444–445 (2007) 387–390.
[6] B. Ravel, M. Newville, J. Synchrotron Radiat. 12 (2005) 537–541.
[7] J.J. Rehr, R.C. Albers, Rev. Mod. Phys. 72 (2000) 621–654.
[8] P. Martin, S. Grandjean, M. Ripert, M. Freyss, P. Blanc, T. Petit, J. Nucl. Mater. 320 (2003) 138–141.
[9] J. Rodriguez-Carjaval, Abstracts of the satellite on powder diffraction of the XV congress of the IUCr, 127, Toulouse, France, 1990.
[10] S.D. Conradson, B.D. Begg, D.L. Clark, C. Den Auwer, M. Ding, P.K. Dorhout, F.J. Espinosa-Faller, P.L. Gordon, R.G. Haire, N.J. Hess, D. Webster Keogha, G.H. Lander, D. Manara, L.A. Morales, M.P. Neu, P. Paviet-Hartmann, J. Rebizant, V.V. Rondinella, W. Runde, C. Drew Tait, D.K. Veirs, P.M. Villella, F.J. Wastin, J. Solid State Chem. 178 (2005) 521–535.
[11] E.D. Crozier, J.J. Reher, R. Ingalls, in: D.C. Koningsberger, R. Prins (Eds.), Chemical Analysis, X-Ray Absorption: Principles, Applications, Techniques of EXAFS, SEXAFS and XANES, vol. 92, Wiley-Interscience, New York, 1988, pp. 373–442.
[12] F. Garrido, R.M. Ibberson, L. Nowicki, B.T.M. Willis, J. Nucl. Mater. 322 (2003) 87–89.
[13] D.J.M. Bevan, I.E. Grey, B.T.M.J. Willis, J. Solid State Chem. 61 (1986) 1–7.
[14] L. Nowicki, F. Garrido, A. Turos, L. Thomé, J. Phys. Chem. Solids 61 (2000) 1789–1804.
[15] J.M. Haschke, T.H. Allen, J. Alloys Compd. 336 (2002) 124–131.